Toward hidden materials with directional bonds

Shao-Gang Xu,[1,2] Xiao-Tian Li,[3] Zhong-Jia Chen,[4] Chang-Chun He,[5] Chao He,[1] Xiao-Bao Yang,[5] and Hu Xu[1,2,*]

[1]*Department of Physics, Southern University of Science and Technology, Shenzhen 518055, People's Republic of China*

[2]*Quantum Science Center of Guangdong-Hong Kong-Macao Greater Bay Area (Guangdong), Shenzhen 518045, People's Republic of China*

[3]*CAS Key Laboratory of Quantitative Engineering Biology, Center for Genome Engineering and Therapy, Shenzhen Institute of Synthetic Biology, Shenzhen Institute of Advanced Technology, Chinese Academy of Sciences, Shenzhen 518055, People's Republic of China*

[4]*Songshan Lake Materials Laboratory, Dongguan 523808, People's Republic of China*

[5]*Department of Physics, South China University of Technology, Guangzhou 510640, People's Republic of China*

(Received 19 April 2023; revised 28 June 2023; accepted 20 July 2023; published 7 August 2023)

In solid-state physics and materials science, comprehending the configuration space and structure-property relationships of covalent bond systems remains a fundamental challenge due to the high flexibility of local bonding characteristics. To systematically investigate the configuration space of materials featuring directional covalent bonds, we introduce an enumerated growth orientation method. This strategy extends beyond the nucleation process of isolated systems, as it can also be employed to identify hidden polymorphic materials with interesting properties. By applying this approach, we have uncovered a variety of polymorphic graphyne structures possessing desirable properties. Furthermore, our strategy can generate remarkable topological patterns that serve as fundamental components for covalent organic framework design. In summary, our approach offers a promising platform for materials design, which could catalyze the development of functional materials based on covalent bonds.

DOI: 10.1103/PhysRevMaterials.7.084202

I. INTRODUCTION

Solid-state matter is characterized by a unique atomic arrangement and lattice framework, determined by its specific combination of atomic species [1]. In materials science, the structure-property relationship is a fundamental paradigm that seeks to explore the connection between a material's structure and its properties [2]. Therefore, a thorough understanding of a material's structural features is crucial for both advancing fundamental science and promoting technological developments.

The local morphology of a material is predominantly determined by the strength and nature of atomic interactions, driven by chemical bonds between atoms [3]. Unlike materials with ionic or delocalized metallic bonds, covalent bonds exhibit strong directional properties due to the oriented overlapping of orbitals (see Fig. 1). To our knowledge, researchers have utilized the concept of assembling directional local coordination characteristics to design nonmetallic main group allotropes, beyond the major class of organic chemistry. For example, the theoretically predicted two-dimensional (2D) phosphorus porous polymorphs are assembled from phosphorus local motifs [4], and tetrahedral carbon networks are composed of sp^3 hybridized carbon atoms [5]. However, covalent bonding motifs possess flexible spatial distributions and coordination environments, complicating the energy landscape of a given system [6,7]. First-principles optimization can reach the local low-energy basin. For instance, the glasslike energy landscape of boron clusters determines the presence of numerous boron cages [8], and the small energy difference illustrates the natural polymorphism of boron monolayers [9–11]. Exhaustively screening the configuration space of flexible covalent bond systems could uncover hidden structures with desirable properties. However, a practical strategy to achieve this goal remains an open question.

In this paper, we propose an enumerated growth orientation method for exploring the configuration space of materials with directional bonds, using advanced structure recognition techniques and first-principles calculations. This approach can elucidate the initial nucleation process of materials and identify materials with desirable properties. To demonstrate the potential of our method, we examine a family of sp-sp^2 hybridized graphyne structures, revealing several different stable candidates with semiconducting, Dirac-cone features, and second-order topological characteristics. Our success in graphyne structures highlights the significance of our approach in materials design.

II. METHODOLOGY

A. Eigensubspace projection method

To comprehensively depict the atomic configuration surrounding a particular atom i, disregarding chirality, we can construct a decreasing distance matrix

$$\mathbf{D}_i^{\mathrm{dec}} = \begin{bmatrix} z_i & f(d_{ij_1}) & \cdots & f(d_{ij_N}) \\ f(d_{ij_1}) & z_{j_1} & \cdots & f(d_{i_1 j_N}) \\ \vdots & \vdots & \ddots & \vdots \\ f(d_{ij_N}) & f(d_{i_1 j_N}) & \cdots & z_{j_N} \end{bmatrix}, \quad (1)$$

*xuh@sustech.edu.cn

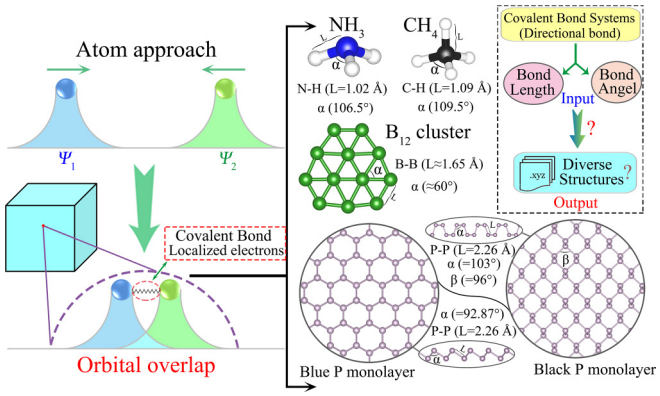

FIG. 1. The schematic diagram of the covalent bonding interaction. The bond lengths (L) and bond angles (α or β) for several typical covalent bond systems. The inset represents the present structural problems in covalent bond systems.

where $j_1, j_2, \ldots, j_N$ are the referenced atoms in the vicinity of atom i within r_{cut}, Z_i is the atomic number (or any other character) of atom i, and $f(d_{ij_1})$ is a decreasing function of the Cartesian distance d_{ij_1} between atoms i and j_1. Such a matrix contains all the geometric information around atom i irrespective of the orientation and atomic ordering (distinct atomic orderings may correspond to permutation similar matrices with no difference in the result).

Through spectral factorization of the decreasing distance matrix, the entire linear space can be decomposed into a direct sum of eigensubspaces. The atomic basis can then be projected onto these eigensubspaces, and the length of the projected vector remains unchanged, irrespective of the choice of eigenvector basis. Consequently, we define the eigensubspace projection array (EPA) of atom i as

$$\mathbf{s}_i = \left(s_i^{\lambda_1}, s_i^{\lambda_2}, \ldots, s_i^{\lambda_s}\right), \tag{2}$$

where $\lambda_1, \lambda_2, \ldots, \lambda_s$ are all the distinct eigenvalues of the decreasing distance matrix arranged in ascending order, and $s_i^{\lambda_k}$ is the norm of the orthogonal projection of atom i on the eigensubspace associated with λ_k. The EPA extracted from the decreasing distance matrix contains the essential information of atom i and serves as a fingerprint.

The EPA in a sense contains the projection information of the atomic basis on the eigensubspaces. Consequently, a visual eigensubspace projection function (EPF) [12,13] can be formulated, where the independent variable represents the proportion of the atomic basis ($S \in [0, 1]$), and the dependent variable Λ represents the eigenvalues associated with the projected eigensubspaces. The difference between atoms i and j in their surrounding structures is defined as

$$\mathbf{d}_{i,j}^{\text{EPF}} = \int_0^1 |\Lambda_i - \Lambda_j| dS, \tag{3}$$

where Λ_i and Λ_j denote the EPFs of atoms i and j, respectively.

B. Computational details

All first-principles calculations were based on density functional theory (DFT) implemented in the Vienna *ab initio* simulation package (VASP) [14]. The electron-ion interactions were described using the projector augmented-wave (PAW) method [15] with a kinetic energy cutoff of 480 eV. For the exchange-correlation interaction energy of electrons, we employed the Perdew-Burke-Ernzerhof (PBE) functional within the generalized gradient approximation (GGA) [16]. To avoid interactions between adjacent periodic images, a vacuum space of 20 Å was included to model the 2D initial structures. All atom positions and lattice constants were fully relaxed until the force on each atom was smaller than 0.01 eV/Å. To investigate the topological properties of the candidates, we constructed maximally localized Wannier functions (MLWFs) using the WANNIER90 package [17,18]. The edge states were calculated employing the iterative Green's function method in the WANNIERTOOLS package [19]. The definition of topological invariants and corner states are provided in the Supplemental Material (SM) [20] (see also Refs. [21–27] therein).

III. RESULTS AND DISCUSSION

The flexible local bonding characteristics of covalent bond systems contribute to the diverse integral structures (e.g., almost equally stable black and blue phosphorus monolayers in Fig. 1) [28]. Finding an effective solution for addressing structural issues in covalent bond systems is crucial for advancing materials science. Inspired by Feynman's fancy of atomic-scale engineering [29], we have extended the idea of manipulating matter atom by atom to materials design. In fact, for systems with directional bonds, we can enumerate the growth orientation to explore all possible candidates. For better understanding, we begin with a simple isolated system with a single type of directional bonds. As shown in Fig. 2(b), based on the nearest-neighbor bonding rule of the triangular lattice, there are eight choices to add the third atom. To filter out equivalent structures for ($n = 3$), we use the 12 symmetry operations (six rotations and six mirror symmetries) of the triangular lattice, resulting in three inequivalent structures. By adding one atom to the isomers of n, we obtain all candidates with $(n + 1)$ atoms, and repeated configurations are removed during structure recognition. We have also explored the configuration space for hexagonal lattice fragments, square lattice fragments, and diamond lattice fragments (see Fig. S1).

Indeed, exploring isolated lattice fragments in 2D materials is critical for comprehensively understanding crystal growth. The high bonding anisotropy in these materials makes their epitaxial growth dependent on the interplay between symmetries of the 2D material and substrate [30]. However, the investigation of initial nucleation growth has been limited by a shortage of samples. For instance, previous studies have only considered the reactivity of C/Si adatoms and dimers on transition metal surfaces [31,32]. We believe that surveying hexagonal lattice fragments can uncover initial self-assembled nucleation behaviors of Xenes (graphene, silicene, germanene, and stanene) [33,34]. Based on triangular lattice fragments, we have demonstrated the structural evolution of boron nanostructures on the Ag (111) surface [35], and the derived stripe pattern has been confirmed by experimental observations [36]. Considering structural stability, the chainlike candidates are always less stable than the close-packed ones,

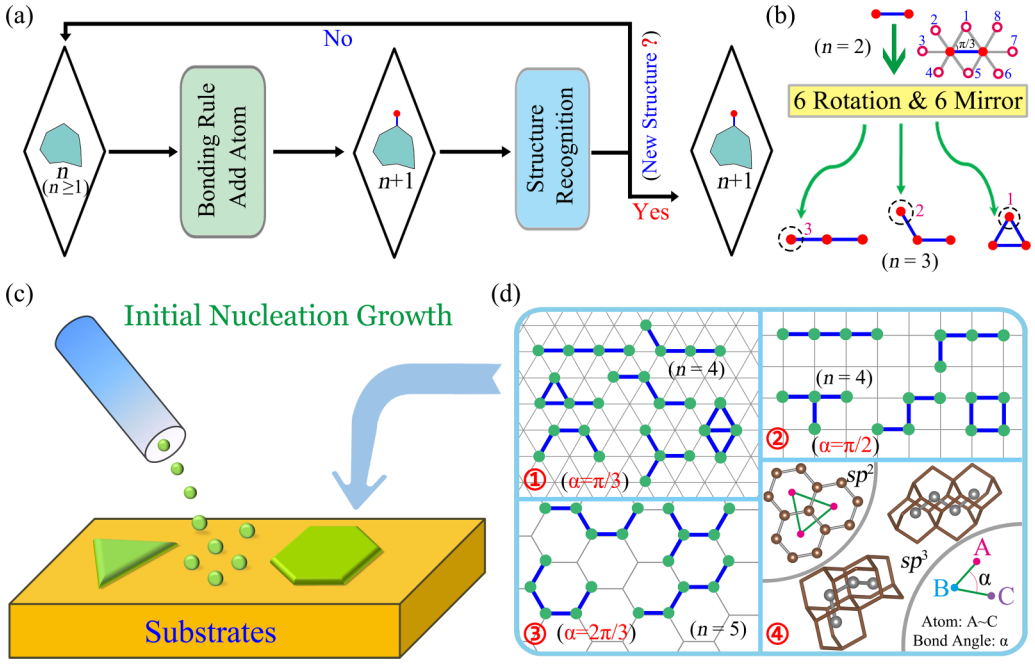

FIG. 2. (a) The flow chart of the enumerated growth orientation method. (b) The growth process of triangular lattice fragments from ($n = 2$) to ($n = 3$). (c) The sketch map of 2D materials growth on substrates. (d) The possible candidates of triangular lattice fragments of ($n = 4$), square lattice fragments of ($n = 4$), hexagonal lattice fragments of ($n = 5$), and two 0D carbon allotropes.

which should be eliminated. However, the less stable chainlike samples may be used as seeds to design other stable nanostructures, such as the chainlike triangular lattice fragments and diamond lattice fragments, which can play a role as center atoms to obtain graphene nanoflakes and diamondoids [37,38] [see Fig. 2(d)].

In most materials, coordination environments are not uniform, as opposed to systems with a single type of directional bonds. Boron monolayers, an emerging star in the field of 2D materials, exhibit unique polymorphic characteristics supported by theoretical calculations and experimental observations [39,40]. Stable boron monolayer candidates exhibit three kinds of coordination numbers (4–6) when considering their local bonding configurations [10]. Similarly, the biphenylene network [41] and the decagonal quasicrystalline surface [42] both exhibit various coexisting directional bonds. Current strategies utilize Archimedean tilings [43,44], which tile the Euclidean plane with regular polygons, to represent these lattices. However, identifying tiles composed of regular polygons only classifies known geometric structures without considering the introduction of interatomic interactions, which is crucial for designing real materials.

The enumerated growth orientation method presents a significant advantage when seeking polymorphic materials that contain multiple types of directional bonds. For the purpose of this study, we focus on a family of representative polymorphic graphyne structures, in which carbon atoms are interconnected by double or triple bonds [45]. Recently, Serafini *et al.* proposed an innovative strategy for designing new graphdiyne materials. They removed edges from the graphene structure and replaced them with linear diacetylenic units, resulting in 17 novel graphdiyne-like structures [46,47]. Moreover, Tao Ouyang *et al.*, utilizing a coordination-constrained search strategy, discovered 48 fresh graphyne allotropes [48]. The versatile sp-sp^2 hybridized C framework in graphyne structures facilitates a broad spectrum of crystal structures, not confined to hexagonal and rectangular symmetries as in previous studies [49–52]. We put forward an enumerated growth algorithm that is based on sp-sp^2 hybridized structures grown on a triangular lattice substrate. The methodology comprises the following: (i) identifying all unique supercells of size n in relation to triangular lattice symmetry to ensure candidate completeness; (ii) generating an initial structure S_1 with a single atom for each unique supercell; (iii) acquiring structures S_{i+1} from parent structures S_i until no additional structures can be found, incorporating the steps of (a) for each unique structure in S_i, determining its viable neighboring sites under the constraint of sp-sp^2 bonding rules, and adding one atom to every possible site to obtain the offspring structures S_{i+1}, (b) removing equivalent structures in S_{i+1} using the EPF, and (c) assessing whether the structures in S_{i+1} have completely bonded under the sp-sp^2 bonding rules; (iv) eliminating output structures that lack an sp^2 hybridized atom or possess an odd number of sp hybridized atoms in the chain (not meeting the π-conjugated condition).

A visual depiction of the growth process is provided in Figs. 3(a) and 4, demonstrating the evolution and representation of the graphyne structures within a specified cell. An initial structure S_1 is first created with a single atom, and this atom C1 interacts with its four equivalent translation copies (a small r_{cut} is used here for clarity), leading to a bifurcation of its EPF. We observe that approximately half of the atomic basis is projected to an eigensubspace associated with an eigenvalue near 4, while the other half is projected to another eigensub-

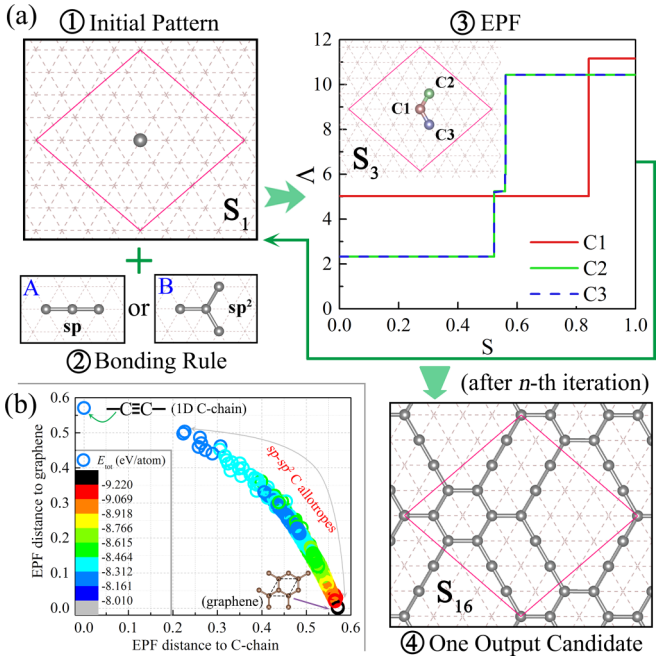

FIG. 3. (a) Illustration of our growth model for graphyne monolayers. For each supercell, an initial structure S_1 is generated with one atom. Based on the sp-sp^2 bonding rule, atoms are added one by one to the neighboring sites of the structure. Repeated structures are eliminated using the EPF method. A structure S_3 is shown in the inset. Note that atoms C2 and C3 have the same EPFs due to their equivalent positions in the periodic structure. Final structures are generated with completely bonded atoms. (b) A plot showing the decreasing EPF distances of the sp-sp^2 C allotropes to two extreme configurations, the 1D C chain, and graphene. The colors of the dots represent the average total energy of the relaxed candidates.

space associated with an eigenvalue near 8. As an additional atom is added to various neighboring sites, two distinct structures are formed, each with markedly different EPFs. It should be noted that the atoms exhibit identical EPFs due to their equivalent surrounding structures. As further atoms are added, the atomic EPFs diverge even more and become varied, enabling us to employ the atomic EPFs to differentiate them (for the purpose of eliminating repeated structures) and to quantify their structural differences. Ultimately, a configuration S_{16} is accomplished with complete bonding under the sp-sp^2 bonding rule.

We discovered 3761 potential, nonequivalent candidates for sp-sp^2 hybridized carbon allotropes ranging from 3 to 55 triangular sites. This was achieved using an atom-by-atom growth process, which includes low-symmetry structures. First-principles calculations were utilized to fully optimize lattice constants and atomic positions for all initial structures. The resulting structures were then assessed in terms of their total energy. An interesting trend emerged: We noticed a decline in EPF distances of the relaxed planar sp-sp^2 C allotropes to two extreme configurations. These configurations consisted of a one-dimensional (1D) C chain with all sp-hybridized C atoms and graphene with all sp^2-hybridized C atoms [refer to Fig. 3(b)]. The most stable candidates encompassed a high ratio of sp^2 hybridized C atoms, and after structural relaxation, 269 candidates transformed into graphene. Notably, many structures formed by the connection of sp^2 hybridized six-membered C rings into infinite one-dimensional stripes were metallic due to delocalized electrons (refer to Fig. S4). Conversely, structures with well-distributed pores surrounded by π-conjugated chains generally exhibited semimetallic or semiconducting properties, which aligns with previous studies of graphyne structures [51,52].

Aiming to balance structural stability and unique properties, we began with isolated closely packed benzene rings and incorporated ethynylene units between the sp^2 hybridized C atoms. This dynamic covalent chemistry approach was previously employed to synthesize the γ-graphyne with long-range order [53]. For this study, we chose seven closely packed six-membered C rings (from one to seven benzene rings) as the center and linked the convex vertex of the center with ethynylene units [refer to Fig. S5(b)]. Using our systematic design algorithm, we constructed 51 typical 2D graphyne structures, enumerating all graphyne phases for a given boundary of a larger-sized supercell. These include the recently synthesized γ-graphyne (GY-1-1) [53] and 6,6,12-graphyne (GY-1-3) [54]. We have named the structures based on the number of included closely packed benzene rings, and the optimized GY-N structures are shown in Figs. S6 and S7.

In comparison to the earlier structures with zero or one benzene ring, including more closely packed benzene rings resulted in more stable candidates. Almost all the designed graphyne monolayers were more stable than the early experimental graphdiyne (GDY) monolayer [55]. When compared to the reported GDY-like structures and other designed GY-like allotropes [46,48], we have identified 20 structures more stable than γ-graphyne [see the yellow shadow in Fig. S5(c)]. This significant advantage in thermodynamic stability suggests a high potential for future fabrication. Additionally, to facilitate comparison with other reported sp-sp^2 carbon allotropes, we have annotated the structures in Table S2 based on the nomenclature defined in the literature [46,52].

Similar to the diverse properties reported in different boron monolayer candidates [56,57], the numerous structures of graphyne monolayers may exhibit a variety of properties. Thus, we calculated the band structures of 51 graphyne monolayers and identified 30 as Dirac semimetals and 21 as semiconductors, with details provided in the SM [20]. While the existence of single and double Dirac-cone features in graphyne structures has been previously reported [51], our calculations confirmed the presence of Dirac cones in stable graphyne structures with a higher proportion of sp^2-hybridized carbon atoms. As shown in Figs. 5(a) and 5(b), GY-4-1 is a stable graphyne structure with low symmetry, and its Dirac points are located along the high-symmetry line connecting the Γ point and other high-symmetry points.

In contrast to the (d-1)-dimensional nontrivial helical edge states in the GY-2-2 graphyne monolayer (see Fig. S11), the hidden second-order topological characters in graphdiyne and γ-graphyne monolayers have recently attracted significant interest [58–62]. Following the parity principle [62], we identified nine second-order topological insulators among the 21 semiconductors we proposed by calculating three Z_2 indices: w_{1a}, w_{1b}, and w_2 (see details in the SM [20]). This approach

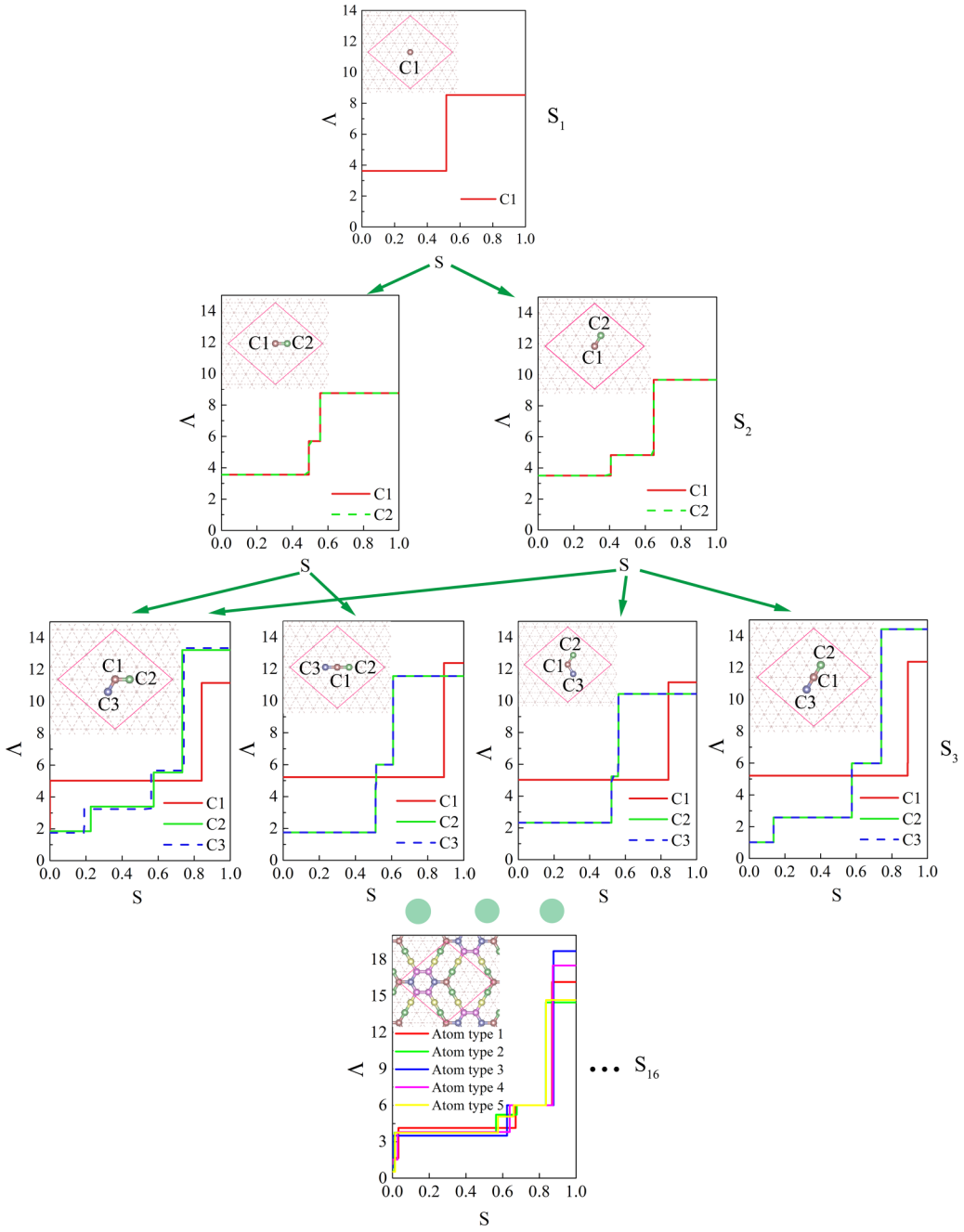

FIG. 4. Structural evolution and EPF representation for graphyne structure growth.

is applicable to semiconducting systems with C_{2z} symmetry and approximate sublattice symmetry. The Z_2 indices were calculated to be $w_{1a} = w_{1b} = 0$ and $w_2 = 1$, indicating the nontrivial band topology. As shown in Fig. 5(d), the stable GY-7-2 structure was found to exhibit gapped trivial edge states that can be approximated by the massive Dirac equation. In this work, we focus on the 2D GY-N systems, and the $(d\text{-}2)$-dimensional protected gapless states should be located at the corner of the 0D nanodisk, which exist at the intersection between two edges belonging to distinct topological phases. Modeling a cluster with 1044 atoms revealed six degenerate corner states in the bulk band gap, with the total charge density distribution shown in Fig. 5(f). These degenerate states, highly concentrated at the corners, are known as the filling anomaly, which is a characteristic feature of second-order topological phases. While strict sublattice symmetry will pin corner states to zero energy, deviations are allowed in realistic materials.

Beyond the 2D case, our strategy can be used to enumerate possible diamondoid frameworks by substituting the center atoms with adamantane units. This led to the discovery of seven diamondoid isomers comprised of 26 carbon atoms (see Fig. S13). Additionally, we constructed several 3D sp^2-sp^3 carbon allotropes using our strategy, out of which we selected two typical semiconducting isomers (see Fig. S14). These examples indicate the broad potential application of our approach.

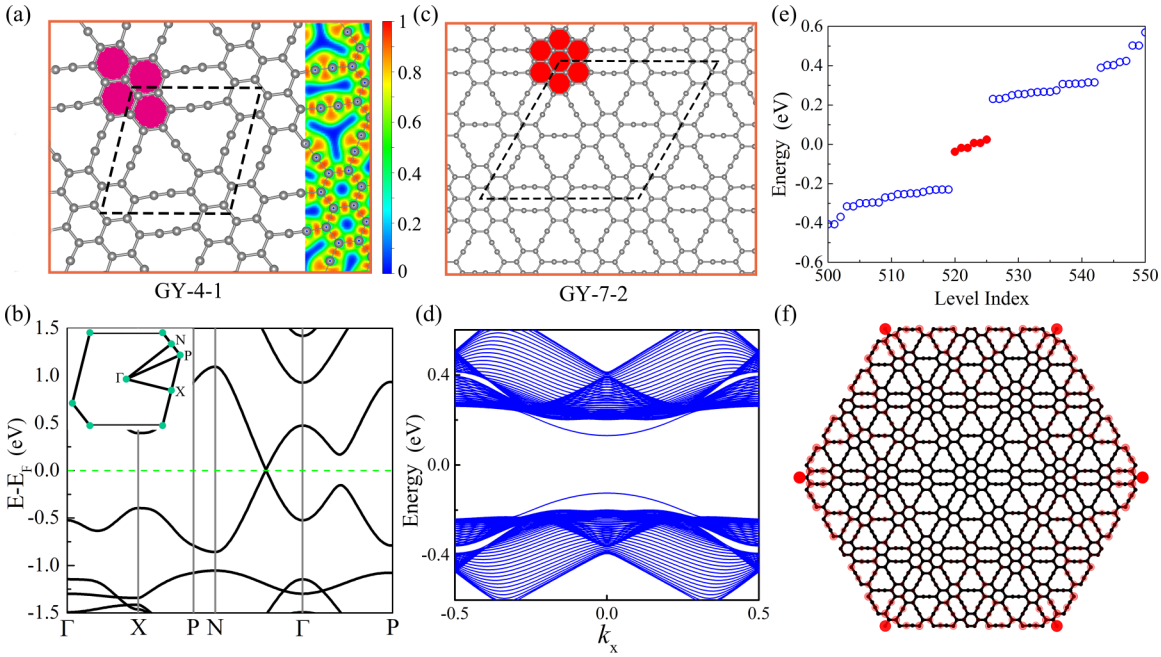

FIG. 5. (a), (c) The geometric structures and 2D electron localization function (ELF) plots for two sp-sp^2 carbon allotropes (GY-4-1 and GY-7-2 monolayers). The black dashed lines represent the unit cells of the corresponding structures. (b) The band structure of the GY-4-1 monolayer. (d) The projected spectra for the k_x edge of the GY-7-2 ribbon. (e) The energy spectrum of the hexagonal-shaped GDY-7-2 nanodisk in (f). (f) The charge distribution of the six zero-energy states of (e), which are localized at corners.

IV. CONCLUSIONS

In conclusion, we have proposed an effective strategy of enumerated growth orientation to explore the configuration space of covalently bonded materials with directional bonds. This approach is applicable across 0D–3D systems and plays a pivotal role in systematically investigating initial nucleation growth, thereby offering significant benefits for materials design. Specifically, we have enumerated all possible nonequivalent candidates of polymorphic graphyne structures, revealing numerous concealed graphyne structures with desired properties. While numerous nonmetal allotropes exhibit less stringent coordination rules, our approach nevertheless yields a wealth of valuable candidates. Beyond the realm of real materials, the topological patterns generated by our algorithm can be leveraged to design various covalent organic frameworks, which are composite products of vertex units and linkage units [63,64]. Our approach provides a universally valuable perspective for seeking out hidden candidates with directional bonds, which may expedite the process of uncovering unknown materials.

ACKNOWLEDGMENTS

This work was supported by the National Key R&D Program of China (Grant No. 2022YFA1403700), the National Natural Science Foundation of China (Grants No. 11974160, No. 12204224, and No. 12247138), the Science, Technology, and Innovation Commission of Shenzhen Municipality (Grant No. RCYX20200714114523069), Guangdong Basic and Applied Basic Research Foundation (Grant No. 2023A1515010734), and Key-Area Research and Development Program of Guangdong Province (Grant No. 2020B010183001). The computer time at the Center for Computational Science and Engineering at Southern University of Science and Technology is gratefully acknowledged.

S.-G.X., X.-T.L., and Z.-J.C. contributed equally to this work.

[1] A. Zunger, Nat. Rev. Chem. **2**, 0121 (2018).
[2] N. Marzari, A. Ferretti, and C. Wolverton, Nat. Mater. **20**, 736 (2021).
[3] F. A. Cotton, G. Wilkinson, C. A. Murillo, and M. Bochmann, *Advanced Inorganic Chemistry* (Wiley, Hoboken, NJ, 1999).
[4] Z. Zhuo, X. Wu, and J. Yang, J. Am. Chem. Soc. **138**, 7091 (2016).
[5] C. He, X. Shi, S. J. Clark, J. Li, C. J. Pickard, T. Ouyang, C. Zhang, C. Tang, and J. Zhong, Phys. Rev. Lett. **121**, 175701 (2018).
[6] A. R. Oganov, C. J. Pickard, Q. Zhu, and R. J. Needs, Nat. Rev. Mater. **4**, 331 (2019).
[7] B. W. B. Shires and C. J. Pickard, Phys. Rev. X **11**, 041026 (2021).
[8] S. De, A. Willand, M. Amsler, P. Pochet, L. Genovese, and S. Goedecker, Phys. Rev. Lett. **106**, 225502 (2011).
[9] E. S. Penev, S. Bhowmick, A. Sadrzadeh, and B. I. Yakobson, Nano Lett. **12**, 2441 (2012).
[10] S.-G. Xu, X.-T. Li, Y.-J. Zhao, J.-H. Liao, H. Xu, and X.-B. Yang, Nanoscale **10**, 13410 (2018).

[11] S.-G. Xu, C.-C. He, Y.-J. Zhao, H. Xu, and X.-B. Yang, Phys. Rev. Mater. **5**, 044003 (2021).

[12] X.-T. Li, X.-B. Yang, and Y.-J. Zhao, J. Chem. Phys. **146**, 154108 (2017).

[13] X.-T. Li, S.-G. Xu, X.-B. Yang, and Y.-J. Zhao, J. Chem. Phys. **147**, 144106 (2017).

[14] G. Kresse and J. Furthmüller, Phys. Rev. B **54**, 11169 (1996).

[15] G. Kresse and D. Joubert, Phys. Rev. B **59**, 1758 (1999).

[16] J. P. Perdew, K. Burke, and M. Ernzerhof, Phys. Rev. Lett. **77**, 3865 (1996).

[17] A. A. Mostofi, J. R. Yates, Y.-S. Lee, I. Souza, D. Vanderbilt, and N. Marzari, Comput. Phys. Commun. **178**, 685 (2008).

[18] N. Marzari, A. A. Mostofi, J. R. Yates, I. Souza, and D. Vanderbilt, Rev. Mod. Phys. **84**, 1419 (2012).

[19] Q. Wu, S. Zhang, H.-F. Song, M. Troyer, and A. A. Soluyanov, Comput. Phys. Commun. **224**, 405 (2018).

[20] See Supplemental Material at http://link.aps.org/supplemental/10.1103/PhysRevMaterials.7.084202 for the topological invariants and corner states, electronic properties analysis for the predicted graphyne phases, and other supplemental figures.

[21] L. Fu and C. L. Kane, Phys. Rev. B **76**, 045302 (2007).

[22] C.-X. Liu, X.-L. Qi, H. Zhang, X. Dai, Z. Fang, and S.-C. Zhang, Phys. Rev. B **82**, 045122 (2010).

[23] J. Ahn, D. Kim, Y. Kim, and B.-J. Yang, Phys. Rev. Lett. **121**, 106403 (2018).

[24] R. Queiroz, I. C. Fulga, N. Avraham, H. Beidenkopf, and J. Cano, Phys. Rev. Lett. **123**, 266802 (2019).

[25] J. Ahn, S. Park, and B.-J. Yang, Phys. Rev. X **9**, 021013 (2019).

[26] W. A. Benalcazar, B. A. Bernevig, and T. L. Hughes, Science **357**, 61 (2017).

[27] N. Mao, R. Li, Y. Dai, B. Huang, B. Yan, and C. Niu, Adv. Sci. **9**, 2202564 (2022).

[28] Z. Zhu and D. Tománek, Phys. Rev. Lett. **112**, 176802 (2014).

[29] R. P. Feynman, in *Miniaturization*, edited by H. D. Gilbert (Reinhold, New York, 1961).

[30] J. Dong, L. Zhang, X. Dai, and F. Ding, Nat. Commun. **11**, 5862 (2020).

[31] H. Chen, W. Zhu, and Z. Zhang, Phys. Rev. Lett. **104**, 186101 (2010).

[32] M. Satta, S. Colonna, R. Flammini, A. Cricenti, and F. Ronci, Phys. Rev. Lett. **115**, 026102 (2015).

[33] A. Molle, J. Goldberger, M. Houssa, Y. Xu, S.-C. Zhang, and D. Akinwande, Nat. Mater. **16**, 163 (2017).

[34] A. J. Mannix, B. Kiraly, M. C. Hersam, and N. P. Guisinger, Nat. Rev. Chem. **1**, 0014 (2017).

[35] S. Xu, Y. Zhao, J. Liao, X. Yang, and H. Xu, Nano Res. **9**, 2616 (2016).

[36] B. Feng, J. Zhang, Q. Zhong, W. Li, S. Li, H. Li, P. Cheng, S. Meng, L. Chen, and K. Wu, Nat. Chem. **8**, 563 (2016).

[37] A. Kuc, T. Heine, and G. Seifert, Phys. Rev. B **81**, 085430 (2010).

[38] Y.-T. Wang, Y.-J. Zhao, J.-H. Liao, and X.-B. Yang, J. Chem. Phys. **148**, 014306 (2018).

[39] Z. Zhang, E. S. Penev, and B. I. Yakobson, Chem. Soc. Rev. **46**, 6746 (2017).

[40] X. Liu, Z. Zhang, L. Wang, B. I. Yakobson, and M. C. Hersam, Nat. Mater. **17**, 783 (2018).

[41] Q. Fan, L. Yan, M. W. Tripp, O. Krejčí, S. Dimosthenous, S. R. Kachel, M. Chen, A. S. Foster, U. Koert, P. Liljeroth *et al.*, Science **372**, 852 (2021).

[42] J. Mikhael, J. Roth, L. Helden, and C. Bechinger, Nature (London) **454**, 501 (2008).

[43] J. A. Millan, D. Ortiz, G. van Anders, and S. C. Glotzer, ACS Nano **8**, 2918 (2014).

[44] F. C. de Lima and A. Fazzio, Nanoscale **13**, 5270 (2021).

[45] J. Kang, Z. Wei, and J. Li, ACS Appl. Mater. Interfaces **11**, 2692 (2018).

[46] P. Serafini, A. Milani, D. M. Proserpio, and C. S. Casari, J. Phys. Chem. C **125**, 18456 (2021).

[47] P. Serafini, A. Milani, M. Tommasini, C. Castiglioni, D. M. Proserpio, C. E. Bottani, and C. S. Casari, Phys. Chem. Chem. Phys. **24**, 10524 (2022).

[48] T. Ouyang, C. Cui, X. Shi, C. He, J. Li, C. Zhang, C. Tang, and J. Zhong, Phys. Status Solidi RRL **14**, 2000437 (2020).

[49] R. Baughman, H. Eckhardt, and M. Kertesz, J. Chem. Phys. **87**, 6687 (1987).

[50] N. Narita, S. Nagai, S. Suzuki, and K. Nakao, Phys. Rev. B **58**, 11009 (1998).

[51] D. Malko, C. Neiss, F. Viñes, and A. Görling, Phys. Rev. Lett. **108**, 086804 (2012).

[52] M. Park, Y. Kim, and H. Lee, npj Comput. Mater. **4**, 54 (2018).

[53] Y. Hu, C. Wu, Q. Pan, Y. Jin, R. Lyu, V. Martinez, S. Huang, J. Wu, L. J. Wayment, N. A. Clark *et al.*, Nat. Synth. **1**, 449 (2022).

[54] M. D. Kilde, A. H. Murray, C. L. Andersen, F. E. Storm, K. Schmidt, A. Kadziola, K. V. Mikkelsen, F. Hampel, O. Hammerich, R. R. Tykwinski *et al.*, Nat. Commun. **10**, 3714 (2019).

[55] G. Li, Y. Li, H. Liu, Y. Guo, Y. Li, and D. Zhu, Chem. Commun. **46**, 3256 (2010).

[56] S.-G. Xu, X.-T. Li, Y.-J. Zhao, J.-H. Liao, W.-P. Xu, X.-B. Yang, and H. Xu, J. Am. Chem. Soc. **139**, 17233 (2017).

[57] A. J. Mannix, Z. Zhang, N. P. Guisinger, B. I. Yakobson, and M. C. Hersam, Nat. Nanotechnol. **13**, 444 (2018).

[58] X.-L. Sheng, C. Chen, H. Liu, Z. Chen, Z.-M. Yu, Y. X. Zhao, and S. A. Yang, Phys. Rev. Lett. **123**, 256402 (2019).

[59] B. Liu, G. Zhao, Z. Liu, and Z. Wang, Nano Lett. **19**, 6492 (2019).

[60] C. Chen, W. Wu, Z.-M. Yu, Z. Chen, Y. X. Zhao, X.-L. Sheng, and S. A. Yang, Phys. Rev. B **104**, 085205 (2021).

[61] H. Mu, B. Liu, T. Hu, and Z. Wang, Nano Lett. **22**, 1122 (2022).

[62] E. Lee, R. Kim, J. Ahn, and B.-J. Yang, npj Quantum Mater. **5**, 1 (2020).

[63] Y. Jin, Y. Hu, and W. Zhang, Nat. Rev. Chem. **1**, 0056 (2017).

[64] Y. Lan, X. Han, M. Tong, H. Huang, Q. Yang, D. Liu, X. Zhao, and C. Zhong, Nat. Commun. **9**, 5274 (2018).